Materials Transactions, Vol. 64, No. 9 (2023) pp. 2151 to 2157
Special Issue on Nanostructured Functional Materials and Their Applications IV

Structural, Morphological, Optical Properties and Impedance Analysis of Solution-Processable Ni-Doped CuO Thin Films on ITO/Glass Substrates

La Thi Ngoc Mai[1], Nguyen Van Loi[2], Do Hong Minh[3], Dang Van Thanh[4] and Bui Nguyen Quoc Trinh[1,5,*]

[1]*Faculty of Advanced Technology and Engineering, Vietnam Japan University, Vietnam National University, Luu Huu Phuoc, Nam Tu Liem, Hanoi, Vietnam*
[2]*University of Science, Faculty of Physics, Vietnam National University, 334 Nguyen Trai, Thanh Xuan, Hanoi, Vietnam*
[3]*Faculty of Physical and Chemical Engineering, Le Quy Don Technical University, Building S1, 236 Hoang Quoc Viet, Cau Giay, Hanoi, Vietnam*
[4]*Faculty of Basic Science, University of Medicine and Pharmacy, Thai Nguyen University, 284 Luong Ngoc Quyen Street, Thai Nguyen City, Thai Nguyen Province, Vietnam*
[5]*Key Laboratory for Micro-Nano Technology, University of Engineering and Technology, Vietnam National University, 144 Xuan Thuy, Cau Giay, Hanoi, Vietnam*

Cupric-oxide-based thin films with various amounts of 0, 1, 2, 3, and 4 wt.% Ni doping were, in turn, deposited on ITO/glass substrates via a solution process. The 0.25 M concentrated solutions of copper (II) acetate monohydrate and nickel acetate tetrahydrate were used as starting materials mixed in ethanol solvent, in order to form the precursors. We obtained that the crystalline structure was not affected by the increase in Ni doping concentration as evidenced by X-ray diffraction patterns. The surface morphology observed by scanning electron microscope pointed out the presence of linked-structure nanoparticles. The influence of Ni doping on the optical bandgap width was evaluated by using ultraviolet-visible spectrometry. We found that the optical bandgap should be direct, and it decreased from 2.69 to 2.38 eV for the range doped. Interestingly, we determined the relaxation time of the Ni-doped CuO/ITO/glass structure from measuring the electrochemical impedance spectroscopy, and it was 0.36 s for the undoped film, then gradually decreased to be 0.31, 0.11, 0.1, and 0.04 s with increasing the Ni doping concentration. This achievement result will serve as a foundation for the future photonic researches. [doi:10.2320/matertrans.MT-MG2022027]

(Received March 1, 2023; Accepted March 14, 2023; Published March 31, 2023)

Keywords: *Ni-doped CuO, ITO, solution process, impedance analysis, relaxation time*

1. Introduction

Thin-film oxide materials have attracted the attention of numerous researchers in recent decades because of their intriguing features when compared to bulk structures. Owing to their remarkable optical and electronic properties, these thin films have introduced significant breakthroughs in the fabrication of optoelectronic and photonic devices. In such devices, the numerous *n*-type materials (like ZnO and TiO_2) are used more than *p*-type materials such as CuO and NiO because *n*-type materials have a higher charge mobility efficiency and smaller effective masses for electrons. However, the lack of *p*-type semiconductor materials will make it difficult to develop electronic and photovoltaic devices in the future. It has been well known that the *p*-type semiconductor oxide like CuO exhibits some unique advantages such as high intrinsic carrier concentration, high light absorption coefficient, and low heat emission that could become potential sources for practical applications in solar cells,[1–4] thin film transistors,[5,6] and optical devices.[7] Here, a pure CuO has a direct bandgap of 1.2 eV to 1.9 eV[8,9] with *p*-type conductivity attributed to the generation of cation vacancies in the monoclinic structure.[10] A pure CuO also has a theoretical maximum optical current density of 35 mA/cm^2,[11] implying that it has a big potential for solar applications.

Besides the potential features of pure CuO, many researchers have attempted to change its physical properties such as optical, electrical, and structural characteristics by doping substances to create new compounds. The doping influence of various transition metals such as Ni,[12,13] Zn,[14,15] Fe,[16] and Co[17] has been extensively reported. Among the various transition metals, Ni ions have similar ionic radii to Cu ions[13] and the wide bandgap energy of NiO ranges from 3.6 to 4.0 eV with low electrical resistivity and high thermal stability.[18,19] A destination here is that if the semiconductor with a narrow bandgap is combined to that with a wide bandgap, a new semiconductor might exhibit controllable optical properties, compared to the single one. Therefore, Ni element has been chosen as a dopant for the CuO-based films in our work. There are several studies of the Ni doping influence, for instance, Aakib *et al.*[20] prepared the Ni-doped CuO films on glass substrates and silicon substrates using radio frequency diffraction techniques. The polycrystalline structure of the CuO film is revealed by the impact of Ni ions. Furthermore, as the Ni concentrations increased from 0 to 4.5 at.%, the bandgap energy increased from 1.62 to 1.76 eV, and all the films exhibited *p*-type conductivity. Recently, Baturay *et al.*[13] applied the spin-coating method to fabricate the Ni-doped CuO films on glass substrates. They showed that Ni doping decreased the bandgap energy of the films from 2.03 eV to 1.96 eV, and it simultaneously increased the electrical conductivity of the films. Also, it was revealed that the Ni doping changed the surface morphology in the presence of nanoparticles on the membrane surface. Dolai *et al.*[21] used the sol-gel technique to fabricate the Ni-doped CuO thin films which were contained 0.1, 1.9, and 4.7 at.% Ni doping, verifying that the Ni ions mostly contained in the Ni^{2+} state in the films. The ferromagnetic behavior was also observed at 300 K, and the magnetization

*Corresponding author, E-mail: trinhbnq@vnu.edu.vn

decreased with increasing the temperature. Das and Mitra[12] deposited the Ni-doped CuO thin films by successive ion layer adsorption and reaction (SILAR) method and analyzed the influence of Ni ions on the impedance properties of the films. There, the impedance spectroscopy conducted an increase in the AC conductivity and the resistivity component of the dielectric constant after doping 6% Ni, that made the carrier density enhanced. Electrochemical Impedance Spectroscopy (EIS) is a technique that applies the frequencies of AC characteristic to elucidate the electrical properties of semiconductor materials. The EIS technique can analyze the relationship between electrical and chemical factors such as doping concentration or defect distribution. Moreover, impedance spectroscopy is widely used in the study of the mechanism of photonic devices such as organic solar cells and silicon solar cells.[22,23] However, it has been also possible to study electronic and ionic transport and recombination processes.

As reported that there are many different physicochemical methods used to fabricate the Ni-doped CuO thin films, including sol-gel,[13,19,24] successive ion layer adsorption and reaction (SILAR) technique,[12] and sputtering technique.[20] In this work, we fabricated pure CuO and Ni-doped CuO thin films by solution-processed method because of outstanding benefits such as low cost and fast processing time. In addition, this method allows the formation of uniform films on conformal substrates. Despite the fact that a lot of studies had investigated the photoelectric properties of CuO-based films, a few of them had considered the use of impedance measurement for a systematic and deep discussion. Hence, we focused on the characterization of structural, surface morphological, and optoelectric properties of the Ni-doped CuO thin films, which were deposited on the ITO/glass substrates. Interestingly, we analyzed the impedance performance to determine the relaxation time after forming the *p-n* junction between the Ni-doped CuO film and the ITO layer.

2. Experimental Procedures

2.1 Substrates cleaning

In the first step, the ITO substrates were cleaned with the organic solvents such as acetone and ethanol for 5 min each, and then rinsed with the deionized water for 5 min under the assistance of ultra-sonication cleaner to remove any organic contaminants before deposition. In the second step, the ITO substrates were surface-treated with a cold plasma flow for 10 min to enhance the adhesion between the precursors and the substrates when spin coating.

2.2 Precursors forming

The precursor solutions were synthesized from copper acetate monohydrate and ethanol solvent, which kept a constant concentration of 0.25 M. As a stabilizer, we added monoethanolamine (MEA) to the solution produced. The molar ratio of Cu^{2+} solution to MEA was fixed at 1:2, and the nickel acetate tetrahydrate was utilized as the Ni dopant source with various Ni doping concentrations of 1, 2, 3, and 4 wt.%. The solution was stirred at 75°C for an hour on the hot plate to reach a complete dissolvability.

2.3 Thin films depositing

For the deposition step, the precursor solution was covered onto the ITO/glass substrates using a spin coater with the speed of 1500 rpm for 40 s. Next, the Ni-doped CuO thin films were heated to 90°C for 3 min in air to release the remaining solvent. Finally, the films were heated at 300°C for 30 min in air to make them crystallized.

2.4 Characterization

X-ray diffraction (XRD, Bruker, D2 phase) was used to investigate the crystalline structure of whole the films. The surface morphology was observed using a scanning electron microscopy (SEM, JEOL JSM-IT100). The optical absorption was recorded using UV-Vis spectroscopy (UV 2450-PC, Shimadzu). The electrical properties and the relaxation time of Ni-doped CuO thin films were analyzed using a three-electrode system with EIS. In this measurement, the Ni-doped CuO thin films were used as the working electrode (*WE*). Meanwhile, a silver chloride (AgCl/Ag) electrode and platinum sheet electrode were used as the reference electrode (*RE*) and counter electrode (*CE*), respectively, as seen in Fig. 1. The electrolyte used here was a 0.5 M Na_2SO_4 solution.

3. Results and Discussion

3.1 XRD analysis

Figure 2 shows the XRD patterns of CuO and Ni-doped CuO films deposited on the ITO/glass substrates. We can observe that the position of received peaks was mostly matching with that of the standard ITO peaks. When the diffractive patterns were zoomed in, the peaks of the CuO phase appeared at two main positions of 35.95° and 38.18°, but their intensity was weak and not sharp. It means that, probably, the crystalline microstructures of CuO films were primarily formed on the ITO/glass substrates rather than

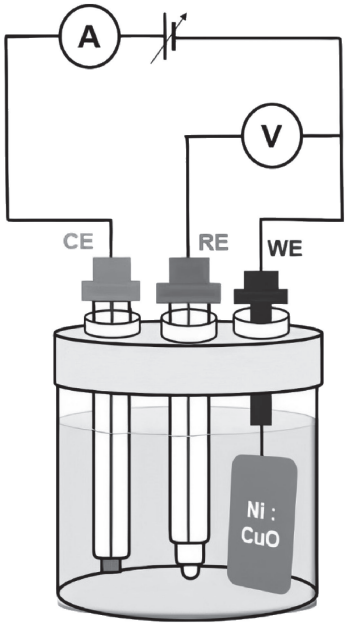

Fig. 1 Schematic drawing of the three-electrode measurement system. Here, *WE*, *RE*, and *CE* are abbreviated for working electrode, reference electrode, and counter electrode, respectively.

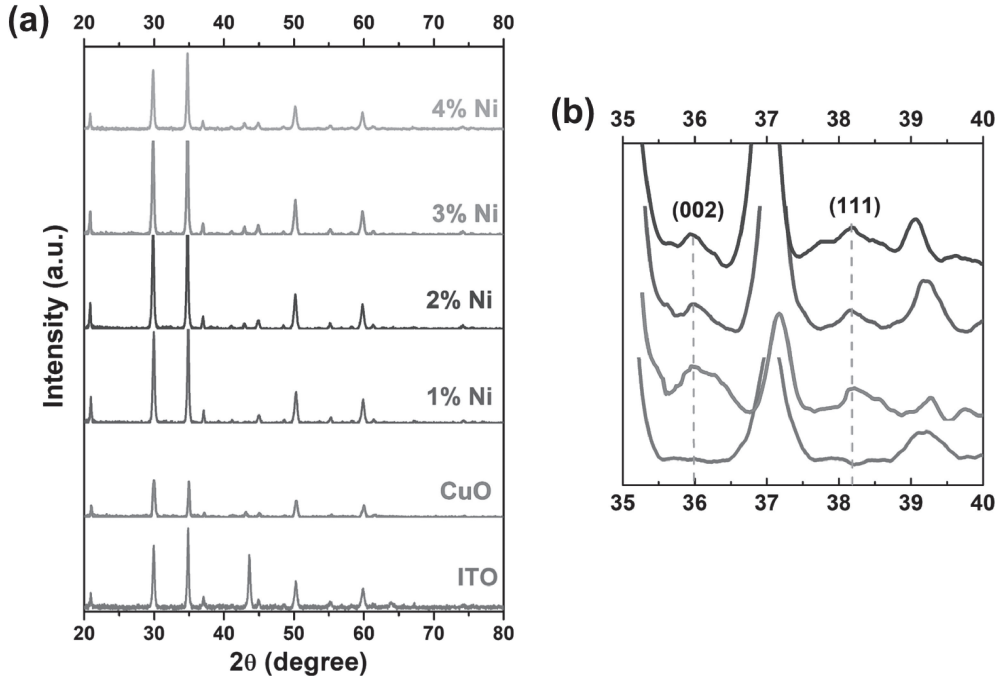

Fig. 2 XRD patterns of all Ni-doped CuO thin films (a), and the enlarged diffraction patterns in the range of 35° to 40° (b).

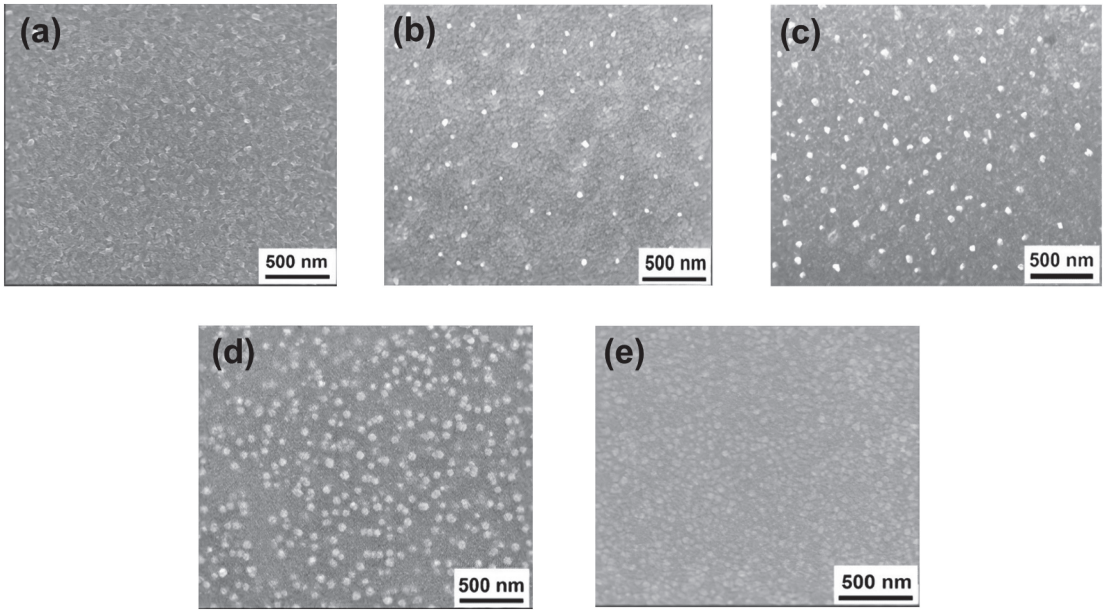

Fig. 3 SEM micrographs of the Ni-doped CuO thin films: (a) 0 wt.%, (b) 1 wt.%, (c) 2 wt.%, (d) 3 wt.%, and (e) 4 wt.% Ni doping concentration.

others. From Fig. 2, we can also see that no secondary phase (nickel oxide, copper–nickel, nickel-related phase) observed for the Ni-doped CuO films, relating to the effective diffusion of Ni^{2+} in the lattice structure. This is because Cu^{2+} and Ni^{2+} ions have ionic radii of 0.73 Å and 0.69 Å,[13] respectively, which are closed from each other. In other word, the Ni doping does not affect significantly on the crystalline properties of the films as derived.

3.2 Morphological property

Morphological property of the films was studied by SEM technique. The SEM micrographs of Ni-doped CuO films at the concentrations from 0 to 4 wt.% are observed as shown from Fig. 3(a) to 3(e). In Fig. 3(a), the CuO film surface was smooth, and it did not consist of voids or cracks. This outcome had been published by our research group.[5,25] However, the textures of the films changed dramatically when Ni element was introduced, as depicted from Fig. 3(b) to Fig. 3(e). It was obvious that the nanoparticles were individually distributed on the film surface. That is, the Ni^{2+} ions incorporated into the films; and, as increasing of the Ni doping concentration, the density of nanoparticles increased. The presence of nanoparticles on the films was also reported by Baturay *et al.*[13] They suggested that the appearance of the

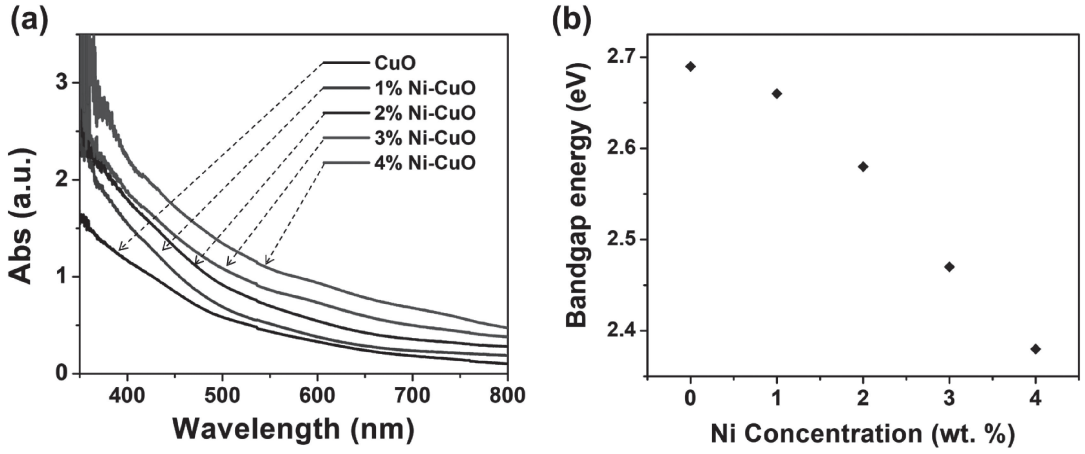

Fig. 4 Optical absorbance spectra (a), and Tauc's plots (b) for the undoped and the Ni-doped CuO thin films.

nanoparticles on film surface enables to contribute an impact on the light absorption and electrical properties for the *p*-type semiconductor layer of the photonic devices. Additionally, the surface structure of CuO film was changed when Ni was added to the CuO structure. In the Ni-doped CuO films, the size of grains for film formation is smaller than that of the film-forming grains on the surface of the CuO film. The grains interconnect more tightly with increasing Ni concentration. This may be due to the difference in ionic radii between Ni and Cu, leading to that Ni ions shrink the crystal structure of Cu and thereby change the size of the grains on the surface of the films. Sayed *et al.*[24] showed that the change in volume of the unit cell when adding Ni to CuO from 81.89 Å^3 to 81.78 Å^3 is due to the difference in ion size, the complexity of the CuO monoclinic crystal structure, and the anisotropic variation in the crystal lattice. That is, as the concentration of Ni increases, the grain size becomes smaller while the density of nanoparticles appearing on the surface increases gradually. In Fig. 3(e), the appearance of nanoparticles with denser density on the surface is observed and almost obscures the underlying film, and thus the surface of the 4% Ni-doped CuO film is smoother than others.

3.3 Optical property

The optical property of the Ni-doped CuO films was extracted from UV-Vis absorbance spectra in the range of 350 to 800 nm, as shown in Fig. 4(a). The films started an absorption at the wavelength of 800 nm, and the absorption of photo energy was highest at the near-ultraviolet region. We found that the absorption of the films increased with the increase of Ni doping concentration. This could be because of an increase in the density of hole states with increasing the Ni doping concentration. According to Fig. 3, the SEM micrographs of the films showed the formation of nanoparticles on the film surface, which became denser and denser with the Ni doping concentration, leading to absorb the light more strongly, compared to the smooth surface of the pure CuO film, as can be seen in Fig. 4(a). The achievement result should be an advantage of the Ni doping to capture the maximum amount of incident light. To further investigate the optical property, the value of bandgap energy, E_g, was calculated using Tauc relation as follows.

Table 1 Series resistance and bandgap energy of the Ni doped CuO thin films.

Ni doping concentration (wt.%)	0	1	2	3	4
R_1 (Ω)	16.37	30.97	41.83	360.02	49.96
R_2 (KΩ)	23.28	40.58	2.04	29.53	13.09
E_g (eV)	2.69	2.66	2.58	2.47	2.38

$$\alpha h\nu = A(h\nu - E_g)^m \quad (1)$$

Where A is the energy-independent constant, α is the absorption coefficient of the material, and $h\nu$ is the incident photo energy, and m is the constant with values of 1/2, 1/3, 2, and 3 depending on direct allowed, direct forbidden, indirect allowed, and indirect forbidden transition, respectively.[26] The value of m is 1/2 since the CuO-based thin film is a direct transition gap material.[13]

Figure 4(b) shows the dependence of bandgap energy on the Ni doping concentration. From this figure, we can see that the E_g values for all films decreased from 2.69 eV for the undoping to 2.66, 2.58, 2.47, 2.38 eV corresponded to 1, 2, 3, 4 wt.% Ni doping concentrations as shown in Table 1. Basing on the tendency, one can be convinced the Ni ions diffused or interspersed into the copper ion sites in the CuO lattice, resulting in the increase of donor density and the additional number of energy levels near the valence-band edge of the CuO bandgap, which caused the bandgap energy to be decreased. With the increase of Ni doping concentration in the CuO nanostructures, Baturay *et al.*[13] reported that the bandgap energy decreased from 2.03 eV for the pure CuO film to 1.96 eV for the 6% Ni doped film. The presence of doping elements or lattice defects (e.g. Cu^+ and O vacancies) had been evidenced to affect the band energy.[27] As a result, the Ni doping changed the bandgap energy of the films slightly, which can make the Ni doped CuO thin films to have wide applicability in photonic devices.

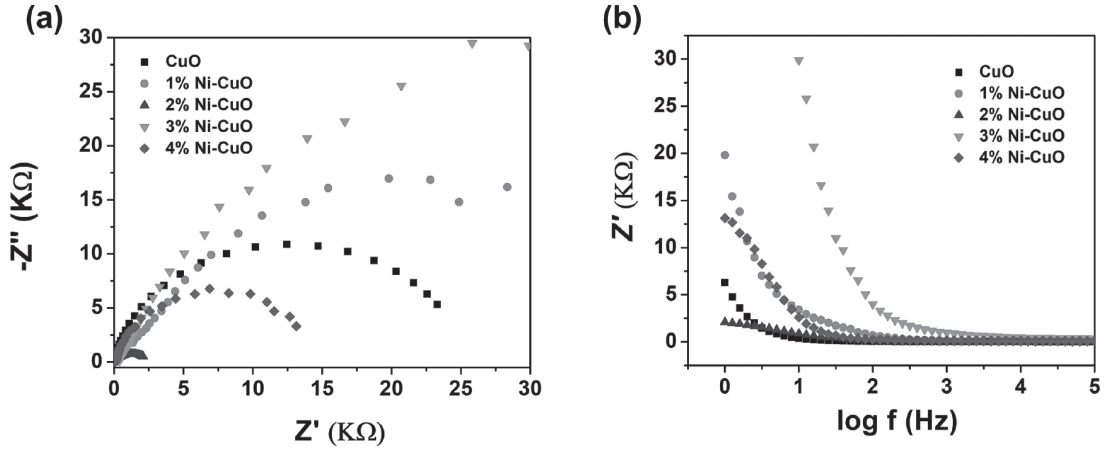

Fig. 5 Nyquist plot (a) and variation in the resistive part Z' with frequency (b) for the undoped and the Ni-doped CuO thin films.

3.4 Impedance analysis

The electrical properties and the relaxation time were carried out from the EIS measurement. The formation of *p-n* junction between the Ni-doped CuO film and the ITO layer plays important roles in the photonic applications. Hence, the EIS technique will result in the charge transport through the relaxation time parameter, in order to assess the relevance of the *p-n* junction. The EIS technique is used to separate resistance and capacitance as real and imaginary components in impedance analysis, providing a clear information about material natures. Impedance data appeared as a series of semicircles indicating electrical phenomena caused by a bulk-grain material or a grain boundary.[28] The complex impedance plots of Z' versus Z'' for 0, 1, 2, 3, and 4 wt.% Ni-doped CuO thin films were shown in Fig. 5(a). In this situation, Z' represented the complex impedance's resistive component, while Z'' contained its capacitive component. Figure 5(a) showed single semicircle plots of the impedance measurement in dark conditions, revealing that the films contributed to the total conductivity, and they took a part of the electron transfer (transport) mechanism. The diameter of the semicircles changed when Ni ions were added, showing that Ni ions had affected this alteration. The formation of series resistance is due to the resistance of the metal-semiconductor contact or the lateral resistance of the ITO-grid contact. In theory, when the resistance of the conductor is too high, the short circuit current will be reduced.

Figure 5(b) shows the frequency variation of the resistance (Z') for the Ni-doped CuO/ITO with various Ni doping concentration. It can be seen that the high-frequency region was related to a low resistance. Once frequency increased, carrier hopping (electrons) increased, resulting in an increase in electrical conductivity. On the other hand, Z' changed with the amount of doping variation because of the change in barrier height with doping.[28]

Figure 6 shows the dependence of relaxation time on Ni doping concentration. The insert of Fig. 6 illustrated a circuit characteristic of the films, whose equivalent circuit formed consists of R_1 as the resistance associated with solution, wires; R_2 is the recombination resistance; constant phase element (*CPE*) is the capacity of the double electric layer at the solid/electrolyte interface; and, Z_W is Warburg diffusion.[29] *CPE* is present when there are the non-uniform surface, surface roughness, and porosity of the electrode in the system. The value of resistors, R_1 *and* R_2, determined from the Nyquist plot were listed in Table 1. The diameter of the semicircle in Fig. 5(a) represents the charge transfer resistance (R_2) between the sample/electrolyte interface, which controls the electron transfer kinetics of the redox reaction at the electrode surface. The 1% Ni-doped CuO film exhibits poor charge transfer kinetics compared with the doped samples as shown in Table 1, and the 2% Ni doped in the film exhibits the lowest charge transfer resistance compared to other films. Therefore, the EIS results that ensure efficient charge separation were achieved with a small amount of 2% doping Ni. Besides, the variation of these resistance values can also be influenced by the film surface morphology such as surface roughness, and results in different exposure to the electrolyte solution. However, this change has not corresponded to the appearance of nanoparticles and the increase of nanoparticle density on the surface as observed from Fig. 3. Conventionally, the characteristic values of *p-n* junction such as a short circuit current, an open-circuit voltage, a fill factor, and a lifetime

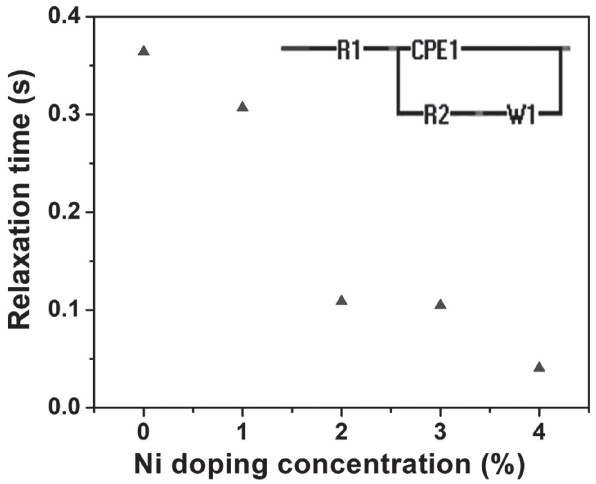

Fig. 6 Dependence of the relaxation time on the Ni doping concentration according to the impedance measurement analysis. The inserted figure is a model of equivalent circuit simulated from impedance data.

need to be determined; however, the relaxation time parameter has not been investigated much and deeply for the Ni doped CuO thin films up to now. The thermal and electrical transport properties are related to the relaxation time. Here, the relaxation time is the time when electrons collide with impurities or oscillations due to lattice defects, and when the electrons return to the equilibrium state due to the inactive electric field.[30] The relaxation time is closely related to the electrical conductivity. Khatavkar *et al.* proposed that the relaxation time was the lifetime of minority carrier in the absence of traps for the copper indium gallium selenide (CIGS) solar cells.[31] In addition, *CPE* is often used to describe relaxation processes, such as charge transfer at heterogeneous electrode surfaces or carrier transport in the amorphous semiconductors.[32] The relaxation time of the carriers (τ) can be expressed by using the relationship as found in the Ref. 33).

$$\tau = R_2 * CPE \quad (2)$$

It should be noticed that eq. (2) does not contain the information of recombination lifetime.[34] According to the result in Fig. 6, the relaxation time of the films decreased as the Ni doping concentration increased. In particular, the relaxation time value of the films was 0.36 s for the pure CuO film, and then decreased to 0.31, 0.11, 0.1, 0.04 s when adding 1, 2, 3, and 4 wt.% Ni doping. One noted that the relaxation time values of Ni-doped CuO/ITO are in the seconds range. The relaxation time process takes place at least two-time scales in semiconductors and electrochemical cells. The faster process (femtoseconds) represents electronic transitions during recombination, while the slower process (microseconds to seconds) is used to study electron and ion conductions at material interfaces, as well as the lattice polarization or dipole rearrangements.[32,35,36] Therefore, we found that the relaxation time resulted from this study is in the slow time range of the charge transfer process. Furthermore, Ni element is used as a dopant which exhibits ferromagnetic nature. Kutes *et al.*[37] pointed out that the ferromagnetic effect causes polarization of the lattice, thereby altering the scale time of the carriers. This experiment was performed under dark conditions, and it was also reported by Chen *et al.*[36] that the slow relaxation time does not depend on the energy of the light. Pockett *et al.*[38] explained the anion or cation vacancies can migrate to form double ion layers at the perovskite/electron and perovskite/hole extraction interfaces as measured by the EIS instrument. However, the impedance analysis on the relaxation time parameters of CuO materials is still uncommon, especially when doping Ni into the pure CuO thin films. Chaudhary *et al.*[39] fabricated Co-doped CuO materials at various Co concentrations and used dielectric measurements to calculate the relaxation time in the order of picoseconds. Othonos *et al.*[40] also determined the relaxation time of CuO nanowires in the picoseconds scale time by studying the temporal behavior of ultrafast time-resolved absorption obtained from simultaneous measurements of time-resolved transmission and reflection. From the result of relaxation time calculated by impedance analysis, we believe that the Ni-doped CuO films fabricated will be suitable to grow the *p*-type layer in the Ni-doped CuO/ITO/glass structure as a single *p-n* junction because of the slow time range, found in this study.

From Fig. 6, we can see the relaxation time decreased with the Ni doping concentration, that is, with the electrical conductivity. This is reasonable since the relaxation time is proportional to the electrical resistivity. The decreasing behavior of relaxation time is relatively matched with the SEM data shown in Fig. 3, because the nanoparticle coverage increased as the Ni doping concentration increased, and the inter-grain gap was filled. Besides, it can be seen that as the Ni doping concentration increased, the bandgap energy decreased and the electrical conductivity increased when using the sol-gel technique to fabricate Ni-doped CuO thin films, as shown in Fig. 4. All the results revealed that the Ni doping through the sol-gel method, in this work, improved the photoelectric properties of CuO-based films, and promoted the development of high efficient photonic devices.

4. Conclusion

In summarization, the Ni-doped CuO thin films with Ni doping concentrations ranged from 0 to 4 wt.% were successfully deposited onto the ITO/glass substrates using a solution-based technique. XRD analysis showed no secondary phase of Ni ions in the structure of films fabricated, and the Ni ion doping had not changed the crystalline structure of the films as well. SEM micrographs of the films indicated that increasing the Ni doping concentration affected the surface morphology of films. The bandgap energy of the films varied from 2.69 to 2.38 eV with increasing the Ni doping concentration. The slow relaxation time of the Ni-doped CuO/ITO layout was determined to be 0.36 s for the case of pure CuO film, but gradually decreased with increasing the Ni doping concentration because the film resistance is proportional to the relaxation time. Eventually, it is convinced that EIS analysis must be a useful tool to estimate the relaxation time of carriers, and it can be used to evaluate the promising formation of a junction between the Ni-doped CuO film and the ITO layer.

Acknowledgment

This work is fully supported by the project with the code number of VJU.JICA.21.03, from Vietnam Japan University, under Research Grant Program of Japan International Cooperation Agency.

REFERENCES

1) A. Kaphle, E. Echeverria, D.N. Mcllroy and P. Hari: RSC Adv. **10** (2020) 7839.
2) M. Dahrul, H. Alatas and Irzaman: Procedia Environ. Sci. **33** (2016) 661.
3) O. Daoudi, Y. Qachaou, A. Raidou, K. Nouneh, M. Lharch and M. Fahoume: Superlattices Microstruct. **127** (2019) 93.
4) H. Absike, Z. Essalhi, H. Labrim, B. Hartiti, N. Baaalla, M. Tahiri, B. Jaber and H. Ez-Zahraouy: Opt. Mater. **118** (2021) 111224.
5) B.N.Q. Trinh, N.V. Dung, N.Q. Hoa, N.H. Duc, D.H. Minh and A. Fujiwara: Thin Solid Films **704** (2020) 137991.
6) K.C. Sanal, L.S. Vikas and M.K. Jayaraj: Appl. Surf. Sci. **297** (2014) 153.

7) G. Shetty, V. Crasta, R. Kumar, R.K.R. Bairy and P.S. Patil: Opt. Mater. **95** (2019) 109218.
8) Y. Wang, S. Lany, J. Ghanbaja, Y. Fagot-Revurat, Y.P. Chen, F. Soldera, D. Horwat, F. Mücklich and J.F. Pierson: Phys. Rev. B **94** (2016) 245418.
9) R. Sahay, J. Sundaramurthy, P.S. Kumar, V. Thavasi, S. Mhaisalkar and S. Ramakrishna: J. Solid State Chem. **186** (2012) 261.
10) C. Wang, X.Q. Fu, X.Y. Xue, Y.G. Wang and T.H. Wang: Nanotechnology **18** (2007) 145506.
11) S. Masudy-Panah, R.S. Moakhar, C.S. Chua, H.R. Tan, T.I. Wong, D. Chi and G.K. Dalapati: ACS Appl. Mater. Interfaces **8** (2016) 1206.
12) M.R. Das and P. Mitra: J. Sol-Gel Sci. Technol. **87** (2018) 59.
13) S. Baturay, A. Tombak, D. Kaya, Y.S. Ocak, M. Tokus, M. Aydemir and T. Kilicoglu: J. Sol-Gel Sci. Technol. **78** (2016) 422.
14) M. Nesa, M. Sharmin and A. Bhuiyan: Mater. Sci. Semicond. Process. **122** (2021) 105479.
15) P. Samarasekara, P.G.D.C.K. Karunarathna, H.P. Weeramuni and C.A.N. Fernando: Mater. Res. Express **5** (2018) 066418.
16) P. Revathi, V.M. Nikandan, P. Ezhilmathi, V.U. Shankar, P. Suganya and K. Krishnasamy: Asian J. Chem. **32** (2020) 2763.
17) H.Z. Asl and S.M. Rozati: J. Electron. Mater. **49** (2020) 1534.
18) T.H. Fang and K.J. Chen: Mater. Trans. **48** (2007) 471.
19) Ha.L. Chen, Y.M. Lu and W.S. Hwang: Mater. Trans. **46** (2005) 872.
20) H. El Aakib, J.F. Pierson, M. Chaik, H. Ait Dads, C. Samba Vall, A. Narjis and A. Outzourhit: Spectrosc. Lett. **54** (2021) 487.
21) S. Dolai, S.N. Sarangi, S. Hussain, R. Bhar and A.K. Pal: J. Magn. Magn. Mater. **479** (2019) 59.
22) G. Garcia-Belmonte, A. Guerrero and J. Bisquert: J. Phys. Chem. Lett. **4** (2013) 877.
23) I. Mora-Seró, G. Garcia-Belmonte, P.P. Boix, M.A. Vázquez and J. Bisquert: Energy Environ. Sci. **2** (2009) 678.
24) H. Khmissi, A.M.E. Sayed and M. Shaban: J. Mater. Sci. **51** (2016) 5924.
25) H.Q. Nguyen, D.V. Nguyen, A. Fujiwara and B.N.Q. Trinh: Thin Solid Films **660** (2018) 819.
26) N. Koteswara Reddy and K.T. Ramakrishna Reddy: Thin Solid Films **325** (1998) 4.
27) Y. Hong, J.W.Y. Lam and B.Z. Tang: Chem. Commun. **29** (2009) 4332.
28) A. Azam, A.S. Ahmed, M. Chaman and A.H. Naqvi: J. Appl. Phys. **108** (2010) 094329.
29) A.R.C. Bredar, A.L. Chown, A.R. Burton and B.H. Farnum: ACS Appl. Energy Mater. **3** (2020) 66.
30) J. Yu, L. Xu, B. Zhang and W. Jie: Mater. Res. Express **7** (2020) 015901.
31) S. Khatavkar, K. Muniappan, C.V. Kannan, V. Kumar, K.L. Narsimhan, P.R. Nair, J.M. Vasi, M.A. Contreras, M.F.A.M. Van Hest and B.M. Arora: Phys. Status Solidi A **215** (2018) 1700267.
32) E. von Hauff: J. Phys. Chem. C **123** (2019) 11329.
33) K. Guruprasad, G. Marappan, S. Elangovan, S.V. Jayaraman, K.K. Bharathi, G. Venugopal, C.D. Natale and Y. Sivalingam: Nano Express **1** (2020) 030020.
34) L. Bertoluzzi, R.S. Sanchez, L. Liu, J.-W. Lee, E. Mas-Marza, H. Han, N.-G. Park, I. Mora-Sero and J. Bisquert: Energy Environ. Sci. **8** (2015) 910.
35) E. von Hauff: J. Phys. Chem. C **123** (2019) 11329.
36) X. Chen, Y. Shirai, M. Yanagida and K. Miyano: Phys. Chem. Chem. Phys. **20** (2018) 17918.
37) Y. Kutes, L. Ye, Y. Zhou, S. Pang, B.D. Huey and N.P. Padture: J. Phys. Chem. Lett. **5** (2014) 3335.
38) A. Pockett, G.E. Eperon, N. Sakai, H.J. Snaith, L.M. Peter and P.J. Cameron: Phys. Chem. Chem. Phys. **19** (2017) 5959.
39) N.V.P. Chaudhary, J.K. Murthy and A. Venimadhav: Solid State Commun. **247** (2016) 36.
40) A. Othonos and M. Zervos: Nanoscale Res. Lett. **6** (2011) 622.